Photoreduction of Oxoisoaporphines by Amines: Laser Flash and Steady-State Photolysis, Pulse Radiolysis, and TD-DFT Studies

Julio R. De la Fuente,*,† Christian Aliaga,† Cristian Poblete,† Gerald Zapata,‡ Carolina Jullian,† Claudio Saitz,† Alvaro Cañete,§ Gabriel Kciuk,|| Eduardo Sobarzo-Sanchez,⊥ and Krzysztof Bobrowski||

Departamento de Química Orgánica y Fisicoquímica, Facultad de Ciencias Químicas y Farmacéuticas, Universidad de Chile, Casilla 223, Santiago 1, Chile, Departamento de Química Inorgánica y Analítica, Facultad de Ciencias Químicas y Farmacéuticas, Universidad de Chile, Chile, Departamento de Química Orgánica, Facultad de Química, Pontificia Universidad Católica de Chile, Chile, Institute of Nuclear Chemistry and Technology, 03-195 Warsaw, Poland, and Departamento de Química Orgánica, Facultad de Farmacia, Universidad de Santiago de Compostela, Santiago de Compostela, España

Received: February 28, 2009; Revised Manuscript Received: May 11, 2009

Photoreduction of oxoisoaporphine (OIA) (1-aza-benzo-[de]anthracen-7-one) and its 5-methoxy (5-MeO-OIA) derivative by selected amines (two non-α-hydrogen-donating amines (1,4-diaza[2.2.2]-bicyclooctane (DABCO) and 2,2,6,6-tetramethylpiperidine (TMP)) and three α-hydrogen-donating amines (triethylamine (TEA), diethylmethylamine (DEMA), and dimethylethylamine (DMEA))) has been studied in deaerated neat acetonitrile solutions using laser flash and steady-state photolysis. The triplet excited states of OIA and 5-MeO-OIA are characterized by intense absorption maxima located at $\lambda_{max} = 450$ nm and lifetimes of 34.7 ± 0.5 and 44.6 ± 0.4 μs, respectively. In the presence of tertiary amines, both triplets are quenched with a rate constant that varies from the near diffusion limit ($>10^9$ M^{-1} s^{-1}) to a rather low value ($\sim 10^7$ M^{-1} s^{-1}) and shows the expected dependence on the reduction potential for one-electron-transfer reactions. The transient absorption spectra observed after quenching of the respective triplet states are characterized by distinct absorption maxima located at $\lambda_{max} = 480$ and 490 nm (for OIA and 5-MeO-OIA, respectively) and accompanied by broad shoulders in the range of 510−560 nm. They were assigned to either solvent-separated radical ion pairs and/or isolated radical anions. In the presence of α-hydrogen-donating amines these species undergo protonation that leads to the formation of neutral hydrogenated radicals A1H$^\bullet$/A2H$^\bullet$ with two possible sites of protonation, N and O atoms. Pulse radiolysis and molecular modeling together with TD-DFT calculations were used to support the conclusions about the origin of transients.

Introduction

Oxoisoaporphines are a family of oxoisoquinoline-derived alkaloids that have been isolated from Menispermaceae and Sciadotenia toxifera as the sole known natural sources.[1−3] It has been claimed that these compounds could be phytoalexins generated by plants against pathogen infections.[4−7] Some of these compounds derivatives also have DNA binding affinity and cytotoxicity against different tumor cell lines. Moreover, it was found that aminoalkanamido derivatives are selective acetylcholinesterase inhibitors.[8,9]

The only photochemical studies performed so far on these compounds are those for 2,3-dihydro-oxoisoaporphines.[10−12] It was found that the photoreduction mechanism is a stepwise electron−proton−electron transfer process. In a primary step, it involves the radical ion pair complex formation by a single electron transfer from the amine to the excited triplet state of the 2,3-dihydro-oxoisoaorphines. Within the radical ion pair, a proton transfer from the amine radical cation to the radical anion of the 2,3-dihydro-oxoisoaporphine generates the neutral hydrogenated radical ANH$^\bullet$. The latter radical undergoes a second electron transfer from the more reductive imine radical, leading to the N-hydrogenated anion ANH$^-$. On the other hand, an iminium cation of amine gives origin to aldehydes, secondary amines, and diethylaminobutadiene.[10,11]

The photoreduction mechanism was elaborated based on spectral identification of all the intermediates involved in the photoreduction process and analysis of stable photoproducts. Additional support was obtained from semiempirical quantum mechanical calculations using the ZINDO/S method on the PM3-optimized structures of transient species. They allowed spectral assignments of all intermediates involved. Furthermore, the spectral predictions for isolated radical anions (A$^{\bullet-}$), not observable in photochemically induced processes, were confirmed by pulse radiolysis of acetonitrile solutions containing 2,3-dihydro-oxoisoaporphines.[13]

The oxoisoaporphines studied in the current work (Chart 1, 1-aza-benzo-[de]anthracen-7-one (A1) and its 5-methoxy derivative (A2)) are structural analogs of some biologically relevant compounds, namely, phenylphenalenone phytoalexins. They were recognized for their antifungal activity[4−7] attributed either to radicals or singlet oxygen formation or to bacterial DNA intercalation. Therefore, the role of radical species generated by electron transfer from or to phytoalexins is important and cannot be disregarded in their action mechanism.

* To whom correspondence should be addressed. Fax: (56-2)-978-2868. E-mail: jrfuente@ciq.uchile.cl.
† Departamento de Química Orgánica y Fisicoquímica, Universidad de Chile.
‡ Departamento de Química Inorgánica y Analítica, Universidad de Chile.
§ Pontificia Universidad Católica de Chile.
|| Institute of Nuclear Chemistry and Technology.
⊥ Universidad de Santiago de Compostela.

10.1021/jp901877q CCC: $40.75 © 2009 American Chemical Society
Published on Web 06/08/2009

CHART 1

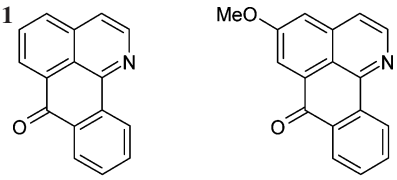

A1 A2

The main difference between 2,3-dihydro-oxoisoaporphines studied previously and oxoisoaporphines studied currently (Chart 1) arises from the aromatic character of the ring-containing N atom in the latter compounds, which causes in consequence their planarity.

Our studies include laser flash photolysis experiments in the presence of various tertiary amines: two non-α-hydrogen-donating amines (1,4-diaza[2.2.2]-bicyclooctane (DABCO) and 2,2,6,6-tetramethylpiperidine (TMP)) and three α-hydrogen-donating amines (triethylamine (TEA), diethylmethylamine (DEMA), and dimethylethylamine (DMEA)). In doing this, it was noticed that depending on the amine either back electron transfer leading to starting substrates or proton transfer leading to metastable photoproducts within the radical ion pair prevailed.

In this work we present laser flash photolysis (LFP) experiments aiming at generation and spectral/kinetic characterization of transients formed in the photoreduction process induced by amines and complemented by pulse radiolysis (PR) experiments and quantum mechanical calculations using the TD-DFT method. These transients show distinctive absorption spectra and evolve kinetically on different time domains, thus allowing their detection and spectral/kinetic characterization by LFP and PR.

In the current work we established a qualitative and partly quantitative picture of the reaction mechanism as a function of amine. These studies provide further evidence for the character of intermediates involved in photoreduction of oxoisoaporphines in the presence of amines. Moreover, they might be also of relevance to electron-transfer processes occurring in phytoalexins and connected potentially with their activity against pathogens.[4,7]

Experimental Section

Materials. Acetonitrile was purchased from J. T. Baker or Merck, HPLC grade, and used as received. Triethylamine (TEA), 2,2,6,6-tetramethylpiperidine (TMP), tribenzilamine (TBzA), triallylamine (TAA), diethylmethylamine (DEMA), dimethylethylamine (DMEA), triphenylamine (TPA), and DABCO were all purchased from Aldrich. All liquid amines were distilled in vacuum, trap-to-trap, sealed into glass tubes at 10^{-4} mm Hg, and stored at −18 °C. Before each experiment, a new tube was opened to ensure the freshness of the amine. Triphenylamine was recrystallized from ethanol, and DABCO was used as received. Solutions of solid amines were prepared immediately before use.

Synthesis of Oxoisoaporphines. A1 and A2 were obtained by the procedure reported by Favre et al.[14] and by Walker et al.[15] and completely characterized as reported previously.[16−18]

Preparation of Solutions. All solutions for laser flash photolysis experiments were prepared with absorbance ≈ 0.4 at an excitation wavelength of 355 nm, and concentration ≈ 0.1 mM. Solutions (3 mL) of oxoisoaporphines in a 10 mm fluorescence quartz cell sealed with a septum were purged for 20 min with N_2 or Ar. Immediately after purging, an aliquot of pure or diluted amine was added through the septum for the quenching or spectral experiments.

Laser Flash Photolysis. Laser flash photolysis experiments were performed with a Q-switched Nd:YAG laser, Quantel Brilliant, with an excitation at 355 nm. The flash photolysis setup was described previously.[11,19,20]

Triplet Quantum Yields. Triplet quantum yields for oxoisoaporphines were measured by energy transfer to β-carotene using benzophenone as a standard. The measurements were made by monitoring the 520 nm ΔOD corresponding to β-carotene triplets[21] of solutions of oxoisoaporphine and benzophenone in acetonitrile, whose absorbances at 355 nm were matched approximately to 0.2. Aliquots of β-carotene in benzene were added to the former N_2-purged solutions to ensure complete energy transfer to β-carotene. ΔOD at 520 nm was measured, measuring the impinging power with a pyroelectric power meter Quantel model MPI-310. Triplet quantum yields (Φ^T) were calculated from the slope of plots of ΔOD_{520} versus laser power, measured with the oxoisoaporphine and benzophenone, using eq 1

$$\Phi^T = (m_{OIA}/m_{Bzph})\Phi^T_{bzph} \quad (1)$$

where m_{OIA} and m_{bzph} are the slopes of the β-carotene triplet absorption at 520 nm sensitized by oxoisoaporphine and benzophenone, respectively, and Φ^T_{bzph} is the triplet quantum yield of benzophenone taken as 1.00.[22]

Pulse Radiolysis. Pulse radiolysis experiments were performed with the INCT LAE 10 linear accelerator with typical pulse lengths of 7−10 ns. The data acquisition system allows for kinetic traces to be displayed on multiple time scales. A detailed description of the experimental setup for optical measurements has been given elsewhere along with the basic details of the equipment and the data collection system.[23,24] The irradiation cell was supplied with a fresh solution by continuous and controlled flow. The dose per pulse, which was determined by thiocyanate dosimetry, was on the order of 18−20 Gy (1 Gy = 1 J kg^{-1}). Radiolytic yields are given in SI units as μmol J^{-1}, i.e., the number of product species in micromoles that are generated for every Joule of energy absorbed by the solution.

All experiments were performed with a continuous flow of sample solutions at room temperature (∼20 °C). Experimental error limits are ±10% unless specifically noted.

All solutions of oxoisoaporphines (0.1 mM) for pulse radiolysis experiments were prepared freshly before experiments in acetonitrile. Solutions were subsequently purged for at least 30 min per 200 mL of sample with the desired gas (Ar or O_2) before pulse irradiation.

Steady-State Photolysis. Solutions (3 mL) of oxoisoaporphine, with absorbances of between 0.20 and 1.40 at 366 nm, were purged with N_2 for 20 min in a 10 mm quartz fluorescence cell sealed with a septum. Immediately after purging, an aliquot of pure or dilute amine was added through the septum. The changes of absorbance with time were followed on the Agilent 8453 diode array spectrophotometer. The solutions were photolyzed directly in the spectrophotometer cell holder with a 150 W Black Ray UV lamp equipped with a 366 nm filter.

Photoconsumption quantum yields (Φ_{pc}) were evaluated using eq 2

$$\Phi_{pc} = (dC/dt)_0/I^\circ(1 - 10^{-Abs}) \quad (2)$$

where $(dC/dt)_0$ is the initial oxoisoaporphine disappearance rate ($M\ s^{-1}$), $I°$ is the photon flux (einstein s^{-1}), and Abs is the absorption at an irradiation wavelength of 366 nm.

Variation in concentration of oxoisoaporphines was evaluated from the absorbances measured at $\lambda = 376$ and 380 nm for A1 and A2, respectively, using eq 3

$$C = C_0(A_0 - A_t)/(A_0 - A_\infty) \quad (3)$$

where C_0 was the initial concentration of oxoisoaporphine and A_0, A_t, and A_∞ are the respective absorbances measured at $t = 0$, t, and ∞, respectively. Photon flux was determined by using Aberchrome 540.[25]

NMR Experiments. NMR measurements were performed with a Bruker Avance DRX-300 (300 MHz) spectrometer. Reactions were carried out by a direct photoreduction of N_2-purged solutions containing a weighted amount of the oxoisoaporphine, typically 1 mg/mL in CD_3CN. Solutions were prepared directly in NMR tubes sealed with septa and N_2 purged for almost 20 min. After purging, an appropriate amount of amine was added in more than 10-fold excess with respect to the oxoisoaporphine. During photoreduction, several ^1H NMR spectra were recorded every few minutes until the spectrum remains unchanged.

Quantum Mechanical Calculations. The geometry of the species studied in this work was optimized by using the DFT method with UB3LYP functional without constraints. Calculations were performed using a 6-311-G(d,p) basis set. The solvent effect was included in calculations by using the continuum solvation model[26] for acetonitrile. DFT stationary points were confirmed as energy minima by frequency analysis of the optimized structures (no imaginary frequencies). The same calculations give also the Gibbs free energy. Electronic transitions of transient species were calculated by single-point calculations using UB3LYP/6-311-G(d,p) with TD = (Nstates = 15) and SCRF = acetonitrile. A similar approach has been applied successfully to several radical systems.[27−29]

Spin contamination was negligible after annihilation of the first spin contaminant for all the studied species; $\langle s^2 \rangle = 0.7500-0.7504$ for radical anion species $A^{\bullet-}$, and the hydrogenated radicals $AH^{\bullet}$. For the triplets $^3A1^*$ and $^3A2^*$ $\langle s^2 \rangle = 2.0005$ and 2.0004, respectively. Therefore, spin contamination should not affect spectral obtained values. Calculations were performed with Gaussian 03[30] in a PC cluster Intel Xeon with 18 processors.

Results

Laser Flash Photolysis and Pulse Radiolysis. ***Triplets: Generation and Spectral/Kinetic Characterization.*** The transient absorption spectra formed 1 μs after the laser pulse excitation of N_2-saturated solutions of oxoisoaporphine (A1) and 5-methoxyoxoisoaporphine (A2) in acetonitrile show distinctive absorption bands with λ_{max} located at 450 nm (Figure 1). These transients decay by first-order kinetics with lifetimes of 34.7 ± 0.5 and 44.6 ± 0.4 μs for A1 and A2 (insert in Figure 1a), respectively.

These absorptions were efficiently quenched by oxygen. The assignment of these species to the triplet state of $^3A1^*$ and $^3A2^*$ was made through energy-transfer experiments employing β-carotene, a well-known triplet quencher, which has a triplet energy of 80 kJ mol^{-1} [31] and an intersystem crossing quantum yield of practically zero.[32] Thus, β-carotene triplet can only be formed through an energy-transfer process from a suitable triplet donor. Triplet quantum yields (Φ^T) of $^3A1^*$ and $^3A2^*$ were measured by energy transfer to β-carotene using benzophenone as a standard (see Experimental Section) and found to be 1 for both oxoisoaporphines. Moreover, the electronic transitions calculated for $^3A1^*$ and $^3A2^*$ using TD-DFT match very well the experimental spectra as far as the position of the absorption maxima and the oscillator strengths (f) are concerned (Figure 1a and 1b). On the basis of the above facts, the absorption bands observed were unequivocally assigned to the T−T absorption of the respective oxoisoaporphines.

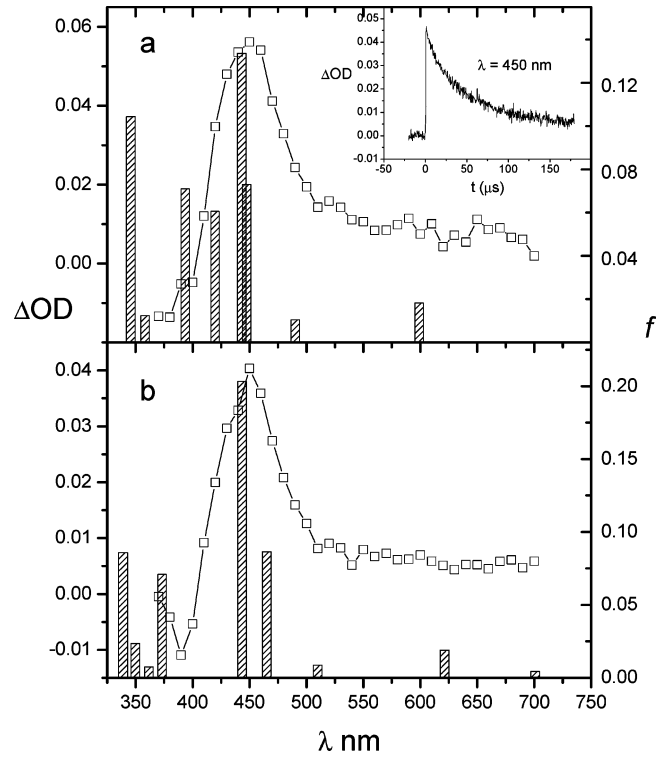

Figure 1. Triplet−triplet transient absorption spectra for (a) 5-methoxyoxoisoaporphine (A2) and (b) oxoisoaporphine (A1). Vertical bars represent the position of the electronic transitions for $^3A2^*$ (Figure 1a) and $^3A1^*$ (Figure 1b) calculated with the TD-DFT method. The height of the bar is proportional to the oscillator strength (f). (Inset) Time profile representing growth and decay of $^3A2^*$ at $\lambda = 450$ nm.

In order to estimate the triplet energy, E^T, for both oxoisoaporphines (A1 and A2), the energy-transfer method was applied. For that purpose, the rates of the quenching of the respective T−T absorption with a selected set of energy acceptors (ranging between 255 and 146 kJ mol^{-1}) were measured. The quenching process of $^3A1^*$ and $^3A2^*$ by selected acceptors can be easily monitored by following the monoexponential decay of both triplets at $\lambda = 450$ nm. Thus, the rate constants for the quenching of $^3A1^*$ and $^3A2^*$ were obtained using eq 4

$$k_{obs} = k_o + k_q[Q] \quad (4)$$

where k_o is the triplet decay rate constant in the absence of quencher, k_q is the triplet rate constant with the quencher, and [Q] is the quencher concentration in mol dm^3. These rate constants have been collected in Table 1S (see Supporting Information). The inset in Figure 2 shows a representative plot for the quenching of $^3A1^*$ by azulene.

The results presented in Table 1S (see Supporting Information) enabled us to define the triplet energy, E^T, for both

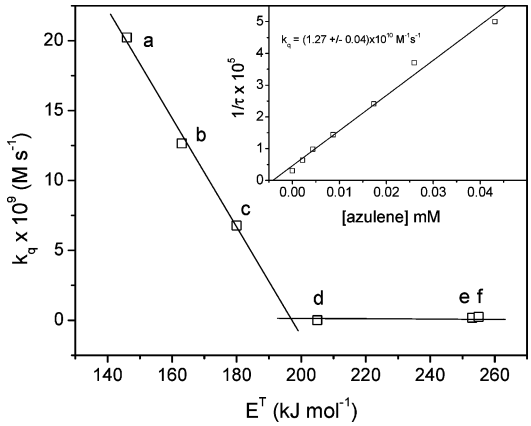

Figure 2. Plot of the quenching rate constants of the excited triplet state of ^{3}A1* versus the triplet energy of (a) perylene, (b) azulene, (c) rhodamine-6G, (d) acridine orange, (e) naphtalene, and (f) quinoxaline.[22] (Inset) Representative plot for the quenching of ^{3}A1* by azulene according to eq 1.

TABLE 1: Quenching Rate Constants of the Excited Triplet States (^{3}A*) Derived from Oxoisoaporphine (A1) and 5-Methoxyoxoisoaporphine (A2) by Selected Amines

amine	reduction potential [V][a] vs NHE[b]	α-H	^{3}A1* k_{ET} [M^{-1} s^{-1}]	^{3}A2* k_{ET} [M^{-1} s^{-1}]
TMP	1.36[33c]	no	8.9×10^6 [2.5×10^7][d]	9.6×10^6
TBzA	1.26[34]	yes	1.1×10^7	1.2×10^7
TAA		yes	1.4×10^7	9.2×10^6
TPhA	1.22[35]	no	9.5×10^7	1.0×10^8
DEMA		yes	1.4×10^9	1.0×10^9
DMEA		yes	1.3×10^9	1.0×10^9
TEA	1.02[36] 1.19[34,37]	yes	1.1×10^9	1.2×10^9
DABCO	0.84[36,37]	no	3.8×10^9 [4.3×10^9][d]	3.2×10^9

[a] The IUPAC convention of writing couples as reduction potentials is recommended. Even though the conversion of amine to amine radical cation involves oxidation, it is preferable to write as the reduction potential of the amine radical cation. The lower value of the reduction potential of the amine radical cation corresponds to increasing ease of oxidation of the amine. [b] Potentials were expressed against NHE by adding 0.242 V to values measured against SCE. [c] Value measured for piperidine.[33] [d] Values measured for 2,3-dihydro-oxoisoaporphine.[11]

oxoisoaporphines (A1 and A2). The respective plot of the quenching rate constants (k_q) of the excited triplet state of A1 versus the triplet energy (E^T) of the quencher is presented in Figure 2. The estimated triplet energies, E^T, for both oxoisoaporphines were found to be equal to 195.5 ± 3 and 193.5 ± 3 kJ mol^{-1} for A1 and A2, respectively.

Quenching of triplet oxoisoaporphines ^{3}A1* and ^{3}A2* by several amines containing α-located hydrogen atoms and without α-located hydrogen atom were performed for different concentrations of amines. Quenching plots based on eq 4 were found to be linear in all cases, from which second-order rate constants shown in Table 1 have been extracted.

The quenching rate constants of the excited triplet states (^{3}A*) derived from oxoisoaporphine (A1) and 5-methoxy-oxoisoaporphine (A2) by selected amines vary from near diffusion limit (>10^9 M^{-1} s^{-1}) to a rather low values (~10^7 M^{-1} s^{-1}) (see Table 1). When non-hydrogen-donating amines such as TMP, TPhA, and DABCO were used as electron donors for ^{3}A*, the triplet quenching rate constants, k_{ET}, shows the expected dependence on the oxidation potentials of the respective amines because

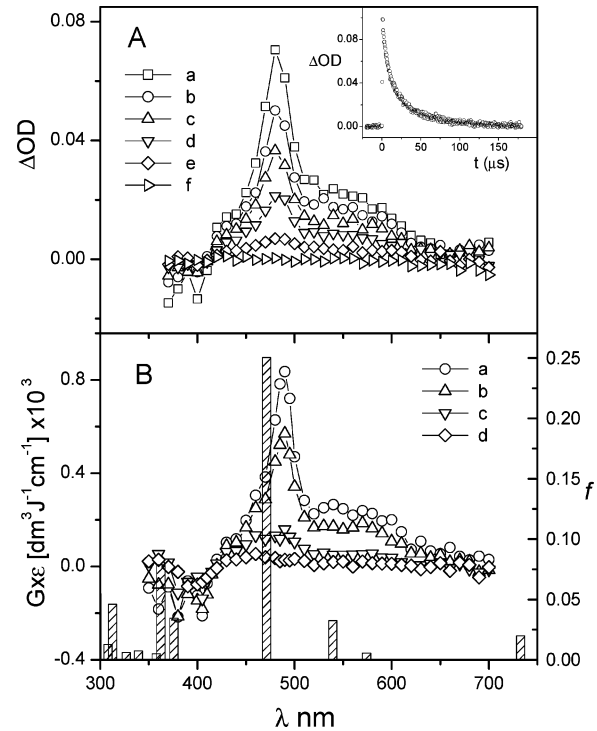

Figure 3. (A) Absorption spectra recorded in N_2-saturated acetonitrile solutions containing 0.1 mM oxoisoaporphine (A1) and 10 mM DABCO. Spectra were taken after the following time delays: (a) (□) 1, (b) (○) 5, (c) (Δ) 10, (d) (▽) 20, (e) (◇) 50, and (f) (>) 150 μs after laser pulse. (Inset) Short time profile representing decay at $\lambda = 480$ nm. (B) Corrected absorption spectra (see explanation in the text) recorded in acetonitrile solutions containing 0.1 mM oxoisoaporphine (A1). Spectra were taken after the following time delays: (a) (○) 200 ns, (b) (Δ) 2 μs, (c) (▽) 8 μs, and (d) (◇) 100 μs after electron pulse. The shaded vertical bars represent the position of the calculated electronic transitions for A1$^{\bullet-}$.

with these amines only a one-electron transfer quenching of ^{3}A is possible, due to the lack of a transferable α-H. A close inspection of the triplet quenching rate constants by hydrogen-donating amines, such as TEA and TBzA, reveals a similar dependence on the oxidation potentials, which strongly leads to one-electron transfer quenching as a dominant process also in the case of α-H-donating amines (see Table 1).

Radical Anions: Generation and Spectral/Kinetic Characterization. A first attempt of generation of the radical anions of the respective oxoisoaporphines (A1$^{\bullet-}$and A2$^{\bullet-}$) was performed in the presence of the non-α-H-donating amines, i.e., TMP and DABCO. When these amines were used as electron donors for ^{3}A1* and ^{3}A2*, new absorption bands appeared in the transient spectra. Figure 3A shows the transient absorption spectra obtained upon laser excitation of oxoisoaporphine (A1) in the presence of excess DABCO (10 mM), in acetonitrile, and recorded at selected times after the laser pulse.

In Figure 3, one can observe that the absorption band corresponding to the triplet of A1 (^{3}A1*) with $\lambda_{max} = 450$ nm is replaced by a new absorption band with $\lambda_{max} = 480$ nm and a pronounced broad shoulder in the range of 500−600 nm already at 1 μs after the pulse (Figure 3A, curve a). This observation is not surprising in view of a high quenching rate constant of ^{3}A1* by DABCO (see Table 1). With the elapse of time this absorption spectrum decayed uniformly at all wavelengths (Figure 3A, curves b−e) without forming any new absorption bands (Figure 3A, curve f). Similar spectral behavior was observed when ^{3}A2* was quenched by excess DABCO (12 mM). A new absorption spectrum was characterized by an

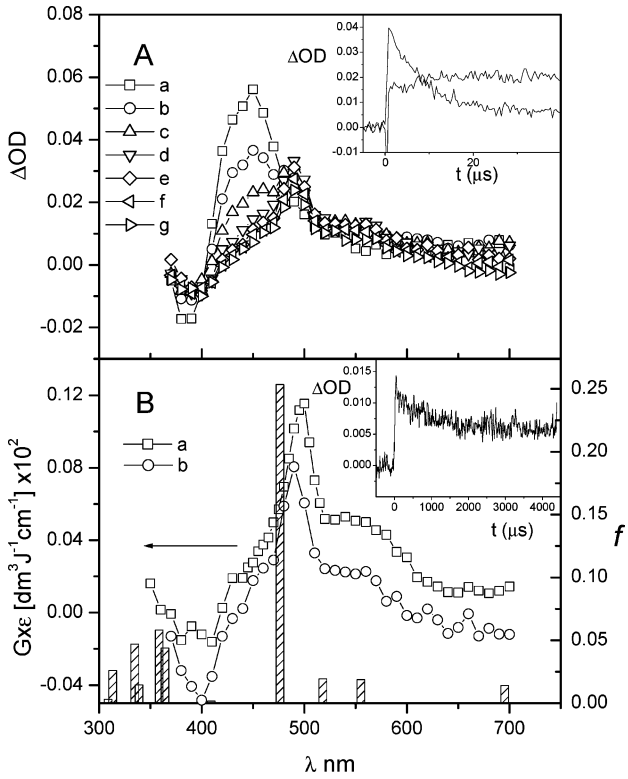

Figure 4. (A) Absorption spectra recorded in N_2-saturated acetonitrile solutions containing 0.1 mM 5-methoxyoxoisoaporphine (A2) and 12 mM TMP. Spectra were taken after the following time delays: (a) (□) 1, (b) (○) 5, (c) (Δ) 10, (d) (▽) 20, (e) (◇) 50, (>) 100, and (g) (<)180 μs after laser pulse. (Inset) Short time profiles representing growth/decay at $\lambda = 480/450$ nm, respectively. (B) (□) Corrected absorption spectrum (see explanation in the text) recorded in acetonitrile solutions containing 0.1 mM 5-methoxyoxoisoaporphine. Spectrum was taken 200 ns after electron pulse. (○) Absorption spectrum recorded in N_2-saturated acetonitrile solutions containing 0.1 mM 5-methoxyoxoisoaporphine (A2) and 12 mM TMP. Spectrum was taken 50 μs after laser pulse. The shaded vertical bars represent the position of the calculated electronic transitions for $A2^{\bullet-}$. (Inset) Long time profile representing decay at $\lambda = 490$ nm in N_2-saturated acetonitrile solutions containing 0.1 mM 5-methoxy-oxoisoaporphine (A2) and 12 mM TMP.

absorption band with $\lambda_{max} = 490$ nm and a pronounced shoulder ranging from 510 to 560 nm which with the elapse of time decayed uniformly at all wavelengths without forming any new absorption bands (data not shown) (see Figure 4A, curves d−g for a similar behavior for A2 in the presence of TMP). These absorptions decay with a lifetime $\tau = 24 \pm 0.5$ μs.

At lower concentration of DABCO (7.6 μM), i.e., at conditions in which the triplet of 5-methoxyoxoisoapophine (^{3}A2*) is still present 1 μs after the pulse, one can observe that the absorption at $\lambda = 490$ nm grows in with first-order kinetics. The precursor of this transient is the triplet of A2 (^{3}A2*) since the decay trace monitored at $\lambda = 450$ nm has a matched rate with the growth rate at $\lambda = 490$ nm ($\tau = 9.7$ μs) (for comparison with TMP, see inset in Figure 4A).

Pulse radiolysis of acetonitrile solutions saturated with argon or oxygen and containing A1 or A2 was performed in order to decide whether the new spectra with $\lambda_{max} = 480$ and 490 nm and a pronounced shoulder at 550 and 540 nm observed in A1 and A2, respectively, can be assigned to radical anions of $A1^{\bullet-}$ and $A2^{\bullet-}$ or to the respective ion−radical pairs $A1^{\bullet-}$/$Amine^{\bullet+}$. In order to eliminate the contribution of radical cation species ($A1^{\bullet+}$ and $A2^{\bullet+}$) in these spectra one has to subtract the absorption spectra obtained in O_2-saturated solutions from the respective absorption spectra obtained in Ar-saturated solutions. Thus, the corrected absorption spectra should correspond mainly to the radical anions ($A1^{\bullet-}$ and $A2^{\bullet-}$) with minor contribution of triplets (^{3}A1* and ^{3}A2*) at shorter times and to the neutral hydrogenated radicals ($A1H^{\bullet}$ and $A2H^{\bullet}$) formed predominantly through protonation by adventitious water at longer times. This approach was successfully applied for 2,3-dihydrooxoisoaporphines.[13]

The corrected absorption spectra recorded in acetonitrile solutions containing A1 at selected times after the pulse are presented in Figure 3B. The spectrum recorded 200 ns (Figure 3B, curve a) is characterized by a distinct absorption band with $\lambda_{max} = 490$ nm and a pronounced broad shoulder ranging from 510 to 610 nm and is very similar in a shape to the spectrum generated photochemically in acetonitrile solutions containing A1 in the presence of DABCO (Figure 3A, curve a). The only difference resides in a small red shift (10 nm) of the location of the maximum of the absorption band. The position of the absorption maximum is in very good agreement with the predicted electronic transition for the radical anion ($A1^{\bullet-}$) calculated by TD-DFT methods (Figure 3B, Table 2S in Supporting Information). With the elapse of time, this absorption spectrum decayed uniformly at all wavelengths for the first microseconds (Figure 3B, curve b). However, contrary to the spectra generated photochemically, at 8 μs after the electron pulse the recorded spectrum started to exhibit different features (Figure 3B, curve c). It becomes broader with weakly developed two absorption maxima. On the basis of our earlier results obtained for 2,3-dihydrooxoisoaporphines, this might suggest the presence of the neutral hydrogenated radicals ($A1H^{\bullet}$) (see Neutral Hydrogenated Radicals: Generation and Spectral/Kinetic Characterization).

Since the quenching rate constant of ^{3}A1* and ^{3}A2* by TMP is lower by more than two orders of magnitude than for DABCO (see Table 1), one could expect better resolution of a direct transformation of ^{3}A1* and ^{3}A2* into respective radical anions of A1 and A2, i.e., $A1^{\bullet-}$and $A2^{\bullet-}$. Figure 4A shows the transient absorption spectra obtained upon laser excitation of 5-methoxyoxoisoaporphine (A2) in the presence of excess TMP (12 mM), in acetonitrile, and recorded at selected times after the laser pulse.

The absorption spectrum recorded 1 μs after the pulse (Figure 4A, curve a) exhibits identical features to that observed for the triplet state of 5-methoxyoxoisoaporphine (^{3}A2*) (Figure 1A). With the further elapse of time, the spectrum started to develop a shoulder on the red side (Figure 4A, curve b), which at 10 μs after the pulse forms a reasonably distinct absorption band with a maximum at $\lambda = 490$ nm (Figure 4A, curve c). This absorption reaches the maximum value at 20 μs (Figure 4A, curve d). At 50 μs after the laser pulse when the 450 nm absorption disappeared completely, the spectrum is characterized by a well-resolved distinct absorption band with $\lambda_{max} = 490$ nm and a pronounced broad shoulder ranging from 510 to 610 nm (Figure 4A, curve e) and is very similar in shape to the spectrum generated photochemically in acetonitrile solutions containing A2 in the presence of DABCO (vide supra). Similarly, as in the presence of DABCO, this absorption spectrum decayed uniformly at all wavelengths without forming any new absorption bands (Figure 4, curves f−g).

Our earlier conclusion that the precursor of this transient is the triplet of A2 (^{3}A2*) was confirmed in the experiments when TMP was a quencher. Again, the decay trace monitored at $\lambda = 450$ nm has a matched rate with the growth rate at $\lambda = 490$ nm (Figure 4A, inset; $\tau = 4.6 \pm 0.3$ μs).

The corrected absorption spectrum generated by pulse radiolysis (vide supra for A1) and recorded in acetonitrile solutions containing A2 at 200 ns after the electron pulse is presented in Figure 4B. The spectrum recorded 200 ns (Figure 4B, curve a) is characterized by a distinct absorption band with $\lambda_{max} = 500$ nm and a pronounced broad shoulder ranging from 510 to 610 nm and very similar in a shape to the spectrum generated photochemically in acetonitrile solutions containing A2 in the presence of TMP (Figure 4B, curve b). The only difference resides, similarly as for A1, in a small red shift (10 nm) of the location of the maximum of the absorption band. The position of the absorption maxima are in a good agreement with the predicted electronic transition for the radical anion ($A2^{\bullet -}$) calculated by TD-DFT methods (Figure 4B, Table 2S in Supporting Information).

At this point we draw attention also to the difference in a kinetic behavior of the transients resulting from a direct triplet quenching (^{3}A1* and ^{3}A2*) by DABCO and TMP and characterized by the absorption maxima located at $\lambda_{max} = 480$ and 490 nm, respectively (Figure 3A, curve a, and Figure 4B, curve b). With DABCO used as a quencher the lifetimes of the transients derived from A1 and A2 were measured as $\tau = 20 \pm 0.7$ (see inset in Figure 3A) and 24 ± 0.0 μs, respectively. Interestingly, with TMP as a quencher, the lifetimes of transients have substantially increased. The lifetimes of the respective transients derived from A1 and A2 were measured as $\tau = 140 \pm 0.0$ μs and 0.9 ± 0.1 ms (see inset for A2 in Figure 4B), respectively.

Neutral Hydrogenated Radicals: Generation and Spectral/Kinetic Characterization. Generation of the radical anions of the respective oxoisoaporphines ($A1^{\bullet -}$and $A2^{\bullet -}$) was performed in the presence of the α-H-donating amines, i.e., TEA, DEMA, DMEA with respect to the expected formation of neutral hydrogenated radicals ($A1H^{\bullet}$ and $A2H^{\bullet}$). This expectation is justified by the former studies when two hydrogen-donating amine (TEA and TBzA) were used for the quenching of 2,3-dihydrooxoisoaporphines triplets.[11]

Figure 5 shows the transient absorption spectra obtained upon laser excitation of 5-methoxyoxoisoaporphine (A2) in the presence of TEA, DEMA, and DMEA ($\sim 10^{-4}$ M) and recorded at selected times after the laser pulse. Similar spectral and kinetic behaviors were observed when ^{3}A1* was quenched by TEA, DEMA, and DMEA (results not shown).

All three amines quenched the triplet of A2 (^{3}A2*) very efficiently with similar rate constants ($\sim 10^{-9}$ M^{-1} s^{-1}) (see Table 1). However, the features of the spectra recorded at the selected times ranging from 1 to 150 μs differ significantly for these amines. A similar spectral and kinetic behavior was observed when ^{3}A1* was quenched by TEA, DEMA, and DMEA (results not shown).

For TEA, the earliest absorption spectrum is that observable 1 μs after the laser pulse and characterized by a broad absorption spectrum with a distinct absorption band with $\lambda_{max} = 410$ and 430 nm and a weaker shoulder ranging from 460 to 500 nm (Figure 5A, curve a). With the elapse of time the spectra recorded at 5, 10, and 20 μs do not change their spectral features significantly in the vicinity of the earlier observed absorption maxima (Figure 5A, curves b−d); however, the second, reasonably distinct absorption band with $\lambda_{max} = 490$ nm appears already 5 μs after the laser pulse (Figure 5A, curve b). Taking into account the fact that the concentration of TEA was equal to 7.6×10^{-5} M and the respective quenching rate constant of ^{3}A2* by TEA (Table 2), one can easily calculate the lifetime of ^{3}A2* of about 11 μs. Therefore, one has to be aware that at

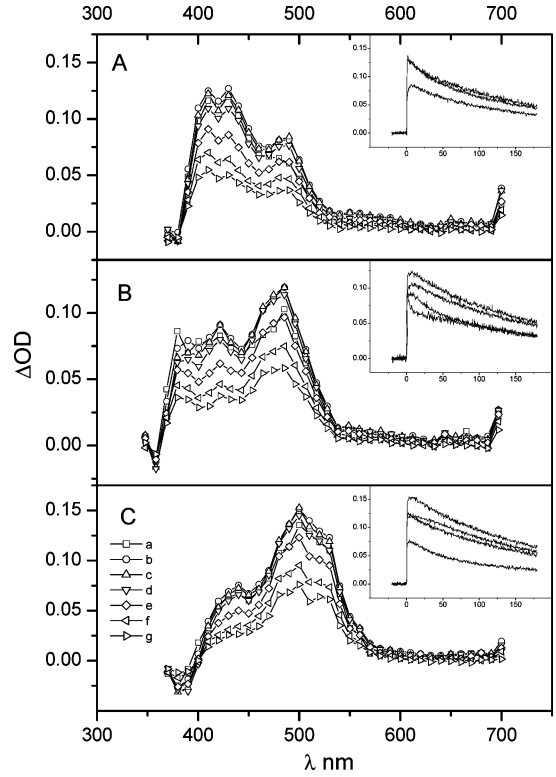

Figure 5. Absorption spectra recorded in N_2-saturated acetonitrile solutions containing 0.1 mM 5-methoxyoxoisoaporphine (A2) and (A) 7.6×10^{-5}M TEA, (B) 9.9×10^{-5}M DEMA, and (C) 1.0×10^{-4} M DMEA. Spectra were taken after the following time delays: (a) (□) 1, (b) (○) 5, (c) (Δ) 10, (d) (▽) 20, (e) (◇) 50, (>) 100, and (g) (<)150 μs after laser pulse. (Insets) Kinetic time profiles recorded at different wavelengths, downward presentation: (A) 410, 430, and 490 nm; (B) 500, 480, 440, and 400 nm; (C) 500, 530, 480, and 440 nm.

short times ^{3}A2* still contributes in the spectra recorded (Figure 5A, curves a−d). Thus, the growth observed at 490 nm within 10 μs after the laser pulse (Figure 5A, inset) can be rationalized as a formation of a transient observed earlier when ^{3}A2* was quenched by the non-α-H-donating amines, i.e., TMP and DABCO (Figure 3A and 4). At longer time scale, starting from 50 μs, the broad absorption spectrum is characterized by three absorption maxima located at $\lambda_{max} = 410$, 430, and 490 nm (Figure 5A, curve e) but however not strongly developed. With the elapse of time, this absorption spectrum started to decay uniformly at all wavelengths (Figure 5A, inset) without forming any new absorption bands (Figure 5A, curves e−g). By analogy with the similar spectral and kinetic features observed with 2,3-dihydrooxoisoaporphines,[11] this absorption could be tentatively attributed to the neutral hydrogenated radical $A2H^{\bullet}$. The positions of the absorption maxima are in good agreement with the predicted electronic transition for the radical $A2H^{\bullet}$ calculated by TD-DFT methods (see Figure 6B and further results of quantum-mechanical calculations and a discussion that concerns another possible structure of neutral hydrogenated radicals).

For DEMA, the earliest absorption spectrum is also that observable at 1 μs after laser pulse and similarly as for TEA characterized by a broad absorption spectrum with a distinct absorption band with $\lambda_{max} = 410$ and 430 nm, in contrast to TEA (Figure 5A, curve a) with the more intense absorption band with $\lambda_{max} = 490$ nm (Figure 5B, curve a). Similarly, as for TEA, the lifetime of ^{3}A2* is about 10 μs, and at short times ^{3}A2* also contributes in the spectra recorded (Figure 5B, curves a−d). Within the first 20 μs after the laser pulse the absorption spectrum does not change much, except in the region where

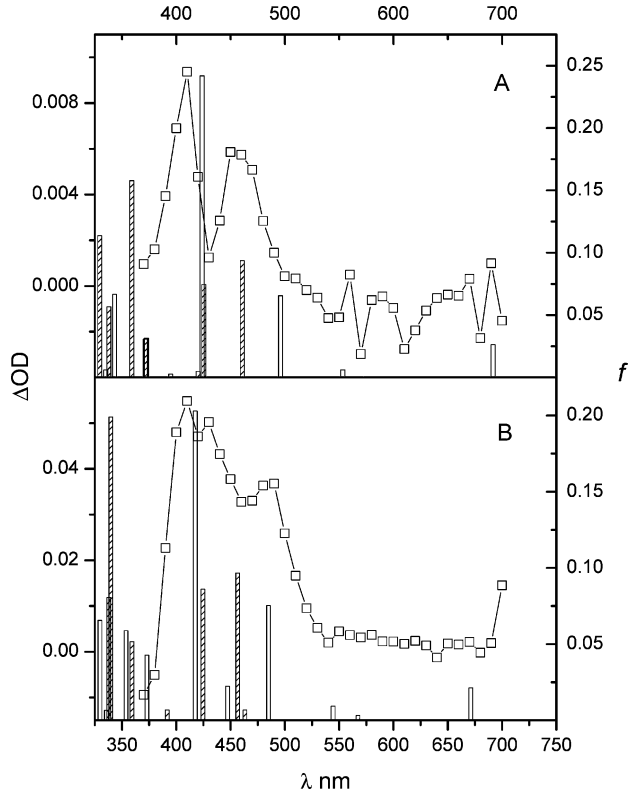

Figure 6. Absorption spectra recorded 150 μs after laser pulse in N_2-saturated acetonitrile solutions containing (A) 0.1 mM oxoisoaporphine (A1) and 2.4×10^{-5} M TEA and (B) 0.1 mM 5-methoxyoxoisoaporphine (A2) and 7.6×10^{-5} M TEA. The shaded vertical bars in A and B represent positions of the calculated electronic transitions for the respective neutral hydrogenated radicals ANH$^{\bullet}$ (white bars) and AOH$^{\bullet}$ (dashed bars).

^{3}A2* absorbs (see the kinetic trace at $\lambda_{max} = 440$ nm, in the inset of Figure 5B). Within the further elapse of time this absorption spectrum started to decay uniformly in the spectrum range around 410 and 430 nm (Figure 5A, curves e−g), without forming any new absorption bands. On the other hand, the absorption band with $\lambda_{max} = 490$ nm decreases faster. Moreover, it has to be noted that the intensity of the absorption band with $\lambda_{max} = 490$ nm, contrary to TEA (Figure 5A, curve g), is higher than the intensity of the absorption band with $\lambda_{max} = 410$ and 430 nm (Figure 5B, curve g). This last observation, taken together with the spectral features of the absorption spectrum observed in a presence of TEA (Figure 5A, curve g) suggests that besides the neutral hydrogenated radicals A2H$^{\bullet}$, a transient resulting from a direct quenching of ^{3}A2* by DEMA also contributes in the spectrum observed at the longest observable time after laser pulse (Figure 5B, curve g). This might indicate that formation of the neutral hydrogenated radicals A2H$^{\bullet}$ is slower when TEA was replaced by DEMA.

Interestingly, for DMEA, the earliest observable spectrum 1 μs after the laser pulse is characterized by the strong absorption band with $\lambda_{max} = 490$ nm and two weaker shoulders located on its both sides (Figure 5C, curve a). The absorption band together with the shoulder on the IR side resembles absorption spectra which were observed earlier when non-α-H-donating amines (DABCO and TMP) were used as quenchers of ^{3}A2* (vide supra). As for the other amines used, taking into account the fact that the concentration of DMEA was equal to 1.0×10^{-4} M and the respective quenching rate constant of ^{3}A2* by DMEA (Table 2), one can easily calculate the lifetime of ^{3}A2* of 10 μs. Therefore, the shoulder seen in the region of 410−450 nm within the first 50 μs (Figure 5C, curves a−e) after laser pulse indicates the presence of ^{3}A2*. With the elapse of time these absorption spectra decayed uniformly at all wavelengths without forming any new absorption bands (Figure 5C, curves b−g).

It is also noteworthy that the absorption band with $\lambda_{max} = 410$ and 430 nm is present when TEA and DEMA were used as quenchers of ^{3}A2* (Figure 5A and 5B) has never been developed (Figure 5C, curves f−g). At this point we draw attention to the similarity in a kinetic and spectral behavior of the transients resulting from a direct triplet quenching ^{3}A2* by the non-α-H-donating amines (DABCO and TMP) and DMEA.

Quantum Mechanical Calculations. ***Excited Triplet States (^{3}A1* and ^{3}A2*).*** The most relevant spectroscopically active electronic transitions along with the oscillator strengths for triplets ^{3}A1* and ^{3}A2* have been calculated as described in the Experimental Section. They are summarized in Table 2S (Supporting Information). The most relevant spectroscopically active electronic transitions for ^{3}A* triplets, and also accessible for experimental observations, are those located at $\lambda \approx 445$ and 465 nm for A1 and $\lambda \approx 395$ and 445 nm for A2 (Table 2S, bold values (Supporting Information)). The electronic transitions with the highest oscillator strengths are in excellent agreement with those experimentally observed (see Figure 1).

Radical Anions (A1$^{\bullet-}$ and A2$^{\bullet-}$). The most relevant spectroscopically active electronic transitions along with the oscillator strengths for radical anions A1$^{\bullet-}$ and A2$^{\bullet-}$ have been calculated. They are also summarized in Table 2S (Supporting Information). The most relevant spectroscopically active electronic transitions for A$^{\bullet-}$ radical anions and also accessible for experimental observations are those located at $\lambda \approx 470$ nm for A1 and $\lambda \approx 475$ nm for A2 (Table 2S, bold values (Supporting Information)). The electronic transitions with the highest oscillator strengths are in reasonably good agreement with those experimentally observed by pulse radiolysis (see Figure 3B, curve a, and Figure 4B, curve a).

Neutral Hydrogenated Radicals (A1H$^{\bullet}$ and A2H$^{\bullet}$). In order to obtain information about potential protonation sites in oxoisoaporphines molecules under study (A1 and A2), PM3 semiempirical quantum mechanic calculations[38] were performed. Spin populations calculated on the optimized radical anions (A1$^{\bullet-}$ and A2$^{\bullet-}$) are treated as rough initial estimations of the possible sites of protonation, thus allowing generation of possible structures of neutral hydrogenated radicals A1H$^{\bullet}$ and A2H$^{\bullet}$. The structures were generated by adding an additional proton to the radical anion structure at the highest spin density sites. The structures of these radicals are shown in Chart 2. Only the H^+ abstracted from the amine radical cations are explicitly shown.

Furthermore, in order to refine calculations, geometries of the neutral hydrogenated radicals (AH$^{\bullet}$) were optimized using the DFT-UB3LYP method with the 6-311G-(d,p) basis set, which enables more reliable estimations of free energies of formation of the respective radicals AH$^{\bullet}$.[28,39] The results of these calculations are summarized in Table 3S (Supporting Information).

The thermodynamically most stable radicals are those protonated on either the N atom (ANH$^{\bullet}$) or the O atom (AOH$^{\bullet}$). The former radicals are more stable by 1.89 and 6.45 kJ mol^{-1} for A1 and A2, respectively (Table 3S (Supporting Information)). Therefore, due to the low difference in energy between ANH$^{\bullet}$ and AOH$^{\bullet}$ radicals, for A1 in particular, one can expect that both radicals are present in equilibrium likely mediated by the amine excess

$$\mathrm{ANH}^{\bullet} \equiv \mathrm{AOH}^{\bullet} \qquad (5)$$

CHART 2: Structures of Possible Neutral Hydrogenated Radicals (AH•) Obtained from PM3 Spin Density Calculations on the Respective Radical Anions (A•−)[a]

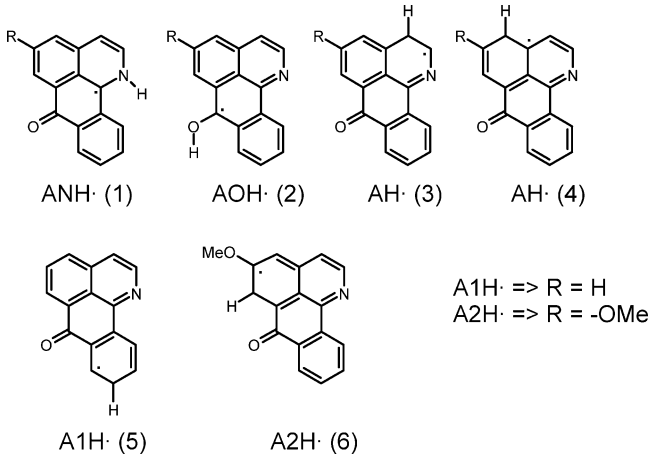

[a] The H atom shown is the additional proton needed to generate AH• from A•−.

The following equilibrium constants at room temperature $K = 0.47$ and $K = 0.077$ for A1 and A2 have been calculated, respectively, taking the respective $\Delta\Delta G°_f$ values from Table 3S (Supporting Information).

The most relevant spectroscopically active electronic transitions for ANH• radicals and also accessible for experimental observations are those located at $\lambda \approx 425$ and 495 nm for A1 and $\lambda \approx 415$ and 485 nm for A2 (Table 3S, bold values (Supporting Information)). On the other hand, the most relevant spectroscopically active electronic transition for AOH• radicals is that located at $\lambda \approx 460$ nm for A1 and A2 (Table 3S, bold values (Supporting Information)).

Taking this set of calculations together ($\Delta\Delta G°_f$ and λ nm (f) from Table 3S (Supporting Information)) one could expect that contribution of the hydrogenated radicals AOH• in the experimentally observed spectrum should be higher for oxoisoaporphine (A1) in comparison to 5-methoxyoxoiso-aporphine (A2).

In order to confront theoretical calculations with experimental observations, the absorption spectra in acetonitrile solutions containing either A1 or A2 and TEA were recorded at a longer time delay after the laser pulse when one might expect only the presence of the hydrogenated radicals (Figure 6).

It is noteworthy that a reasonably good agreement between experimental and calculated spectra for the hydrogenated radicals (A1H• and A2H•) was found. Moreover, the resultant absorption spectra clearly show a contribution of both types of hydrogenated radicals ANH• and AOH•. Furthermore, the distinct absorption band with λ_{max} at 460 nm present in the absorption spectrum recorded in the acetonitrile solution containing A1 (Figure 6A) conforms energetically more favorable formation of AOH• radicals in oxoisoaporphine (A1), in comparison to 5-methoxyoxoisoaporphine (A2). The presence of the AOH• radicals in A2 is manifested only as a shoulder.

Steady-State Photolysis. ***UV−vis Spectroscopy.*** Steady-state photolysis of oxoisoaporphine A1 and 5-methoxy-oxoisoaporphine A2 in acetonitrile in the presence of TEA resulted in the rapid appearance of new absorption bands with maxima located between 250 and 400 nm and a broad band centered at 500 nm. Spectra show apparent isosbestic points located initially at $\lambda = 383$, 399, and 415 nm for A1 and at $\lambda = 350$ and 415 nm for A2 (see insets in Figure 7A and 7B).

For both oxoisoaporphines, A1 and A2, the absorption spectra recover nearly quantitatively to the initial ones when photoreduced samples were stored either in the dark or when O_2 was admitted into reaction cells. During the recovery reaction, the same isosbestic points appear showing a clean back conversion of metastable photoproducts into original oxoisoaporphines (Figure 7). Permanent spectral changes observed <320 nm in the recovered samples were attributed to the amine oxidation products. On the other hand, an absorption recovery to the original absorption of oxoisoaporphines solutions diminishes slightly when the time of photolysis is longer than that needed to reach the maximum of absorption at $\lambda = 500$ nm. This observation is in line with an occurrence of slow secondary photoreaction.

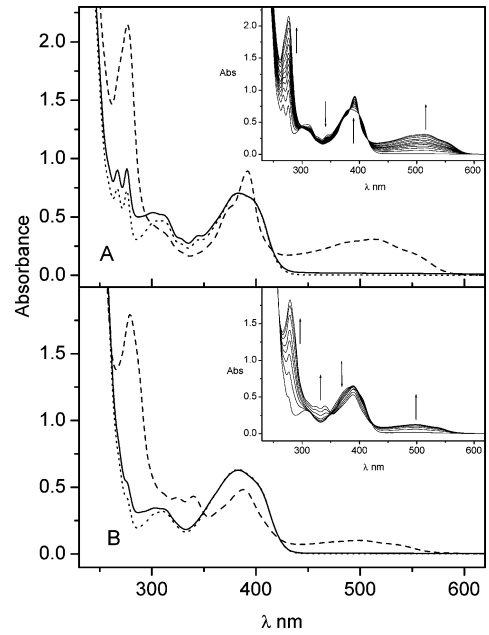

Figure 7. Absorption spectra recorded in acetonitrile solutions containing TEA and (A) oxoisoaporphine (A1), (B) 5-methoxy-oxoisoaporphine (A2) before photolysis (•••), during photolysis when the 500 nm band reaches the maximum (----), and after O_2 admission to the cell (—). Time evolution of the absorption spectra recorded during steady-state photolysis of acetonitrile solutions containing 0.7 mM oxoisoaporphines with [TEA] = 3.0 for A1 (inset in A) and 12 mM for A2 (inset in B). Photolysis was extended to the time when the 500 nm absorption band reaches maximum value.

Analogous spectral behavior was observed with other tertiary amines as DEMA, DMEA, with the appearance of isosbestic points and a recovery of original spectra when air was admitted to the reaction cells.

The photoreaction does not occur with secondary or primary amines like diethylamine or ethylamine since their reduction potentials[37] are probably lower than those of tertiary amines, thus preventing electron transfer to the excited state of oxoisoaporphine.

When photolysis was carried out in the presence of non-α-H-donating amines like DABCO or TMP, spectral changes induced by steady-state photolysis were not observed in spite of the fact that electron transfer took place (see Radical Anions). The lack of photoreduction with these amines confirms unequivocally that a transferable α-hydrogen is needed for the metastable photoproducts formation. These coupled electron proton transfer photoreactions are known to occur in the photoreduction of several heterocyclic compounds.[10−12,19,40−45]

Photoconsumption quantum yields, Φ_{pc}, were estimated from the oxoisoaporphines initial disappearance rate, as described in the Experimental Section. These experiments were performed

in acetonitrile solutions containing 7×10^{-5} M oxoisoaporphine in a large excess of TEA in order to obtain a maximum growth of the 500 nm absorption band. The obtained values were: $\Phi_{pc} = 0.25$ and 0.41 for oxoisoaporphine A1 and the 5-methoxy derivative A2 at [TEA] = 2 and 12 mM, respectively.

NMR Spectroscopy. Direct photoreduction of N_2-purged acetonitrile (CD_3CN) solutions of A1 and A2 in the presence of excess amounts of TEA, DEMA, or DMEA with [amine]/[oxoisoaporphine] > 10 yields complex ^{1}H NMR spectra. The NMR spectra recorded after the first few minutes of photolysis are characterized by the appearance of new signals that could be attributed to metastable photoproducts, likely O- and N-hydrogenated anions AOH^- and ANH^-, and to amines oxidation products (data not shown). Interestingly, ^{1}H NMR spectra of photolyzed samples stored in the dark exhibit a slow recovery to ^{1}H NMR spectra recorded before photolysis, confirming recovery to the starting oxoisoaporphines. This observation is in accordance with recovery of UV−vis spectra observed in photolyzed solutions (vide supra).

The new signals appearing at 4.2, 5.0, and 6.2 ppm were assigned to 1-diethyl-aminobutadiene and those at 2.7 and 1.1 ppm to diethylamine. The quartet appearing near 9.6 ppm was assigned to CHO proton of acetaldehyde. Assignments of signals to diethylamine and acetaldehyde were confirmed by an addition of the respective standards to the photoreaction mixture.

Aldehydes and secondary amines are expected photoproducts during amine oxidation which are formed from the respective iminium cations. Their detection strongly points out that photoreduction occurs by either a sequential electron−proton−electron or electron-hydrogen transfer from the amine to the oxoisoaporphine.[40,46,47] It is worth noting that a similar photooxidation product pattern of TEA was observed during photoreduction of 2,3-dihydrooxo-isoaporphines.[10−12]

Discussion

The present work reports for the first time on spectral and kinetic data regarding the triplets, radical anions, and neutral hydrogenated radicals derived from two oxoisoaporphines, i.e., oxoisoaporphine (A1) and 5-methoxyoxoisoaporphine (A2). In addition, application of pulse radiolysis as a complementary method of generation of radical ions allowed selective generation and observation of radical anions of A1 and A2.

Spectral and Kinetic Characteristics of Transients: Primary Steps of Photoreduction. The absorption maxima assigned to triplets ^{3}A1* and ^{3}A2* are located at $\lambda_{max} = 450$ nm, and they are in excellent agreement with TD-DFT calculations. Their lifetimes are slightly shorter than those derived from 2,3-dihydro-oxoisoaporphines[11] (2,3-DHOIA) being about 35 and 45 μs for ^{3}A1* and ^{3}A2*, respectively. Thus, an aromatic character of the ring-containing N atom does not have much influence on the location of the T−T absorption as well on the lifetimes. However, it has an influence on the triplet quantum yields, Φ^T, which for both ^{3}A1* and ^{3}A2* is equal to 1, larger than those previously reported for 2,3-DHOIA[11] and show that substitution by the methoxy group at position 5 does not affect the efficiency of triplet formation. The estimated triplet energies, E^T, were found to be almost equal, 195.5 and 193.5 kJ mol^{-1} for ^{3}A1* and ^{3}A2*, respectively.

In stark contrast to the 2,3-DHOIA where the experimentally observed absorption bands were unequivocally assigned to the contact ion radical pair complexes[11,13] the absorption spectra generated photochemically in A1 and A2 acetonitrile solutions in the presence of TMP and DABCO (via reaction 6) do not differ substantially from those generated pulse radiolytically in acetonitrile solutions containing A1 and A2 (via reaction 7).

$$^3\text{A1}^*/^3\text{A2}^* + \text{R}_3\text{N} \rightarrow [\text{A1}^{\bullet-}/\text{A2}^{\bullet-}\cdots\text{CH}_3\text{CN}\cdots\text{R}_3\text{N}^{\bullet+}] \rightarrow \text{A1}^{\bullet-}/\text{A2}^{\bullet-} + \text{R}_3\text{N}^{\bullet+} \quad (6)$$

$$\text{A1/A2} + \text{CH}_3\text{CN}^{\bullet-} \rightarrow \text{A1}^{\bullet-}/\text{A2}^{\bullet-} + \text{CH}_3\text{CN} \quad (7)$$

The only difference resides in a small shift (10 nm) of the location of the maxima of the absorption bands. This apparent close match between absorption spectra can be rationalized in the following way. Either in the photochemical system the ion radical pair complexes do not exist as the contact ion radical pairs and are separated by solvent molecules or these complexes are not stable and diffuse apart, forming "isolated" radical anions ($A1^{\bullet-}$, $A2^{\bullet-}$) and radical cations of the respective amine (reaction 6).

The transient absorption spectra observed after quenching of the respective triplet states (^{3}A1* and ^{3}A2*) in the presence of the α-hydrogen-donating amines (TEA, DEMA, DMEA) also confirm formation of the respective solvent-separated radical ion pairs and/or "isolated" radical anions resulting from the electron transfer between triplet states (^{3}A1/^{3}A2) and amines (see reaction 6). However, in contrast to the non-hydrogen-donating amines, their decay is associated with a development of a broad absorption spectrum with three absorption maxima. The spectra were assigned to two forms of the neutral hydrogenated radicals that differ by the protonation site on either the N atom ($ANH^{\bullet}$) or the O atom ($AOH^{\bullet}$) (vide supra). The calculated electronic transitions and thermodynamic stabilities of $ANH^{\bullet}$ and $AOH^{\bullet}$ radicals derived from A1 and A2 are consistent with the features of the respective experimental spectra recorded in acetonitrile solutions containing A1 and A2 (see Figure 6). The existence of two protonation sites in solvent-separated radical ion pair complexes/"isolated" radical anions ($A1^{\bullet-}$, $A2^{\bullet-}$) is an important observation, not previously demonstrated in 2,3-DHOIA systems.[11,13]

The different features of the spectra developed in the presence of various α-hydrogen-donating amines (TEA, DEMA, and DMEA), especially at longer times, and associated with a concomitant decay of the respective solvent-separated radical ion pairs and/or "isolated" radical anions can be rationalized as a statistical control on the proton-donating properties of the respective amine radical cations. This statistical control should depend on the number of methylene groups since their deprotonation is energetically much more favorable than that of methyl groups. This assumption is nicely corroborated by the efficiency of formation of the neutral hydrogenated radicals in the presence of various amines and in the order $TEA^{+\bullet}$ > $DEMA^{+\bullet}$ > $DMEA^{+\bullet}$ (see Figure 5).

Stable Products: Secondary Steps of Photoreduction. The time behavior of the UV−vis spectra together with detection of amine oxidation products by ^{1}H NMR during the photoreduction of oxoisoaporphines in the presence of non-α-hydrogen- and α-hydrogen-donating amines (TEA, DEMA, DMEA) allows concluding that the mechanism of photoreduction of oxoisoaporphines is very similar to that elaborated earlier for photoreduction of 2,3-DHOIA.[10−12] These results suggest that after simultaneous formation of the neutral hydrogenated radicals $A1H^{\bullet}$/$A2H^{\bullet}$ and the neutral C-centered $R_2N-{}^{\bullet}CH-CH_3$ a second electron transfer should take place, resulting ine formation of the metastable ions $A1H^-$/ $A2H^-$ (reaction 8)

$$A1H^{\bullet}/A2H^{\bullet} + R_2N - {}^{\bullet}CH-CH_3 \rightarrow A1H^{-}/A2H^{-} + R_2N^{+}{=}CH-CH_3 \quad (8)$$

The iminium cation formed can react with adventitious water to form the respective aldehyde and secondary amine (reaction 9)

$$R_2N^{+}{=}CH-CH_3 + H_2O \rightarrow CH_3CHO + R_2NH_2^{+} \quad (9)$$

Identification of 1-diethyl-aminobutadiene among other oxidation products of tertiary amines strongly points out that a similar mechanism operates when oxidation of TEA was induced by 2,3-DHOIA derivatives and involves the head-to-tail coupling of the diethylvinylamine intermediate.[10]

Conclusions

Our current findings show that the photoreduction mechanism of oxoisoaporphine (A1) and 5-methoxyoxoisoaporphine (A2) by amines resembles mostly the photoreduction mechanism elaborated on earlier by us for 2,3-dihydrooxoisoaporhine derivatives.[11]

However, some differences exist with respect to the yield and character of intermediates. The primary steps including excitation of the ground state of oxoisoaporphines A1/A2 to the first excited singlet states ^{1}A1*/^{1}A2* followed by intersystem crossing to the lowest excited triplet states ^{3}A1*/^{3}A2* show a substantial increase in the yield of intersystem crossing in comparison to analogous 2,3-DHOIA derivatives.[11,13] Of particular interest is a short-lived intermediate resulting from a single electron transfer between the excited triplet states (^{3}A1* and ^{3}A2*) and amines that was assigned to either solvent-separated radical ion pairs ($A1^{\bullet-}/A2^{\bullet-}\cdots$solvent$\cdots R_3N^{\bullet+}$) or "isolated" radical anions $A1^{\bullet-}/A2^{\bullet-}$). In the presence of non-α-hydrogen-donating amines (TMP, DABCO) these species undergo efficient back electron transfer, leading to the starting substrates. Instead, in the presence of α-hydrogen-donating amines (TEA, DEMA, DMEA), solvent-separated radical ion pairs or "isolated" radical anions undergo protonation that leads to formation of neutral hydrogenated radicals $A1H^{\bullet}/A2H^{\bullet}$. Moreover, there are two possible sites of protonation, N and O atoms resulting in formation of two kinds of C-centered radicals. These radicals probably exist in equilibrium and can be resolved spectroscopically since they are characterized by different electronic transitions.

Molecular modeling together with TD-DFT calculations were used to support the conclusions about the origin of transients. Application of the self-consistent reaction field (SCRF) method with the polarized continuum model (PCM) adequately reproduces experimental absorption spectra. When the solvent effects were not taken into account, the electronic transitions appeared at higher energies (i.e., being blue shifted by about 50 nm). A reasonably good reproducibility of radical anion absorption spectra, using smaller basis, allows disregarding of diffuse functions.

Acknowledgment. We thank FONDECYT grant nos. 1070623 and 7080096 for the financial support which made possible the exchange of scientific visits of J.R.F. in the Institute of Nuclear Chemistry and Technology (Warsaw, Poland) and K.B. in the Universidad de Chile (Santiago, Chile).

Supporting Information Available: Tables for quenching rate constant for selected triplet energy acceptors, TD-DFT-calculated spectra of excited triplet states, calculated formation Gibbs energies, and TD-DFT-calculated spectra for the hydrogenated neutral radical AH$^{\bullet}$. This material is available free of charge via the Internet at http://pubs.acs.org.

References and Notes

(1) Sugimoto, Y.; Babiker, H. A. A.; Inanaga, S.; Kato, M.; Isogai, A. *Phytochemistry* **1999**, *52*, 1431.
(2) Killmer, L.; Vogt, F. G.; Freyer, A. J.; Menachery, M. D.; Adelman, C. M. *J. Nat. Prod.* **2003**, *66*, 115.
(3) Yu, B. W.; Meng, L. H.; Chen, J. Y.; Zhou, T. X.; Cheng, K. F.; Ding, J.; Qin, G. W. *J. Nat. Prod.* **2001**, *64*, 968.
(4) Flors, C.; Nonell, S. *Acc. Chem. Res.* **2006**, *39*, 293.
(5) Lazzaro, A.; Corominas, M.; Marti, C.; Flors, C.; Izquierdo, L. R.; Grillo, T. A.; Luis, J. G.; Nonell, S. *Photochem. Photobiol. Sci.* **2004**, *3*, 706.
(6) Flors, C.; Prat, C.; Suau, R.; Najera, F.; Nonell, S. *Photochem. Photobiol.* **2005**, *81*, 120.
(7) Flors, C.; Ogilby, P. R.; Luis, J. G.; Grillo, T. A.; Izquierdo, L. R.; Gentili, P. L.; Bussotti, L.; Nonell, S. *Photochem. Photobiol.* **2006**, *82*, 95.
(8) Tang, H.; Wang, X. D.; Wei, Y. B.; Huang, S. L.; Huang, Z. S.; Tan, J. H.; An, L. K.; Wu, J. Y.; Chan, A. S. C.; Gu, L. Q. *Eur. J. Med. Chem.* **2008**, *43*, 973.
(9) Tang, H.; Ning, F. X.; Wei, Y. B.; Huang, S. L.; Huang, Z. S.; Chan, A. S. C.; Gu, L. Q. *Bioorg. Med. Chem. Lett.* **2007**, *17*, 3765.
(10) De la Fuente, J. R.; Jullian, C.; Saitz, C.; Neira, V.; Poblete, O.; Sobarzo-Sanchez, E. *J. Org. Chem.* **2005**, *70*, 8712.
(11) De la Fuente, J. R.; Neira, V.; Saitz, C.; Jullian, C.; Sobarzo-Sanchez, E. *J. Phys. Chem. A* **2005**, *109*, 5897.
(12) De la Fuente, J. R.; Jullian, C.; Saitz, C.; Sobarzo-Sanchez, E.; Neira, V.; Gonzalez, C.; Lopez, R.; Pessoa-Mahana, H. *Photochem. Photobiol. Sci.* **2004**, *3*, 194.
(13) De la Fuente, J. R.; Kciuk, G.; Sobarzo-Sanchez, E.; Bobrowski, K. *J. Phys. Chem. A* **2008**, *112*, 10168.
(14) Fabre, J. L.; Farge, D.; James, C. Dibenzo[de,h]quinoline derivatives. In U.S. Patent No 4,128,650, 1978.
(15) Walker, G. N.; Kempton, R. J. *J. Org. Chem.* **1971**, *36*, 1413.
(16) Sobarzo-Sanchez, E.; De la Fuente, J.; Castedo, L. *Magn. Reson. Chem.* **2005**, *43*, 1080.
(17) Sobarzo-Sanchez, E.; Cassels, B. K.; Castedo, L. *Synlett* **2003**, 1647.
(18) Sobarzo-Sanchez, E. Sintesis y Reactividad en el Ambito delas 7H-Dibenzo(de,h)quinolinas. Ph.D. Thesis, Universidad de Chile, 2003.
(19) De la Fuente, J. R.; Cañete, A.; Saitz, C.; Jullian, C. *J. Phys. Chem. A* **2002**, *106*, 7113.
(20) Viteri, G.; Edwards, A. M.; De la Fuente, J. R.; Silva, E. *Photochem. Photobiol.* **2003**, *77*, 535.
(21) Bensasson, R. V.; Land, E. J.; Truscott, T. G. *Excited states and free radicals in biology and medicine. Contributions from flash photolysis and pulse radiolysis*; Oxford University Press Inc.: New York, 1993.
(22) Murov, S. L.; Carmichael, I.; Hug, G. L. *Handbook of Photochemistry*, 2nd ed.; Dekker: New York, 1993.
(23) Mirkowski, J.; Wisniowski, P.; Bobrowski, K. INCT Annual Report: Warsaw, Poland, 2000; INCT: 2001.
(24) Bobrowski, K. *Nukleonika* **2005**, *50*, S67.
(25) Boule, P.; Pilichowski, J. F. *J. Photochem. Photobiol. a: Chem.* **1993**, *71*, 51.
(26) Cossi, M.; Barone, V.; Mennucci, B.; Tomasi, J. *Chem. Phys. Lett.* **1998**, *286*, 253.
(27) Shen, L.; Zhang, H. Y.; Ji, H. F. *Org. Lett.* **2005**, *7*, 243.
(28) Namai, H.; Ikeda, H.; Hirano, T.; Ishii, H.; Mizuno, K. *J. Phys. Chem. A* **2007**, *111*, 7898.
(29) Pal, S. K.; Sahu, T.; Misra, T.; Mallick, P. K.; Paddon-Row, M. N.; Ganguly, T. *J. Phys. Chem. A* **2004**, *108*, 10395.
(30) Frisch, M. J.; Trucks, G. W.; Schlegel, H. B.; Scuseria, G. E.; Robb, M. A.; Cheeseman, J. R.; Montgomery, J. A., Jr., Vreven, T.; Kudin, K. N.; Burant, J. C.; Millam, J. M.; Iyengar, S. S.; Tomasi, J.; Barone, V.; Mennucci, B.; Cossi, M.; Scalmani, G.; Rega, N.; Petersson, G. A.; Nakatsuji, H.; Hada, M.; Ehara, M.; Toyota, K.; Fukuda, R.; Hasegawa, J.; Ishida, M.; Nakajima, T.; Honda, Y.; Kitao, O.; Nakai, H.; Klene, M.; Li, X.; Knox, J. E.; Hratchian, H. P.; Cross, J. B.; Adamo, C.; Jaramillo, J.; Gomperts, R.; Stratmann, R. E.; Yazyev, O.; Austin, A. J.; Cammi, R.; Pomelli, R.; Ochterski, J. W.; Ayala, P. Y.; Morokuma, K.; Voth, P. O.; Salvador, P.; Dannenberg, J. J.; Zakrzewski, V. G.; Dapprich, S.; Daniels, A. D.; Strain, M. C.; Farkas, O.; Malick, D. K.; Rabuck, A. D.; Raghavachari, K.; Foresman, J. B.; Ortiz, J. V.; Cui, Q.; Baboul, A. G.; Clifford, S.; Cioslowski, J.; Stefanov, B. B.; Liu, G.; Liashenko, A.; Piskorz, P.; Komaromi, I.; Martin, R. L.; Fox, D. J.; Keith, T.; Al-Laham, M. A.; Peng, C. Y.; Nayakkara, A.; Challacombe, M.; Gill, P. M. W.; Johnson, B.; Chen, W.; Wong, M. W.; Gonzalez, C. Pople, J. A. *Gaussian 03*, Revision C.02; Gaussian, Inc.: Wallingford, CT, 2004.

(31) Bensasson, R.; Land, E. J.; Maudinas, B. *Photochem. Photobiol.* **1976**, *23*, 189.

(32) Kumar, C. V.; Chattopadhyay, S. K.; Das, P. K. *J. Am. Chem. Soc.* **1983**, *105*, 5143.

(33) Jonsson, M.; Wayner, D. D. M.; Lusztyk, J. *J. Phys. Chem.* **1996**, *100*, 17539.

(34) Mann, C. K. *Anal. Chem.* **1964**, *36*, 2424.

(35) Seo, E. T.; Nelson, R. F.; Fritsch, J. M.; Marcoux, L. S.; Leedy, D. W.; Adams, R. N. *J. Am. Chem. Soc.* **1966**, *88*, 3498.

(36) Nelsen, S. F.; Hintz, T. Z. *J. Am. Chem. Soc.* **1972**, *94*, 7114.

(37) Liu, W. Z.; Bordwell, F. G. *J. Org. Chem.* **1996**, *61*, 4778.

(38) Orozco, M.; Bachs, M.; Luque, F. J. *J. Comput. Chem.* **1995**, *16*, 563.

(39) Klein, E.; Lukes, V. *J. Phys. Chem. A* **2006**, *110*, 12312.

(40) Gorner, H.; Dopp, D.; Dittmann, A. *J. Chem. Soc., Perkin Trans. 2* **2000**, 1723.

(41) Gorner, H.; Elisei, F.; Aloisi, G. G. *J. Chem. Soc., Faraday Trans.* **1992**, *88*, 29.

(42) Fukuzumi, S.; Ohkubo, K.; Tokuda, Y.; Suenobu, T. *J. Am. Chem. Soc.* **2000**, *122*, 4286.

(43) Venkatachalapathy, B.; Ramamurthy, P. *Phys. Chem. Chem. Phys.* **1999**, *1*, 2223.

(44) Peters, K. S.; Kim, G. *J. Phys. Chem. A* **2001**, *105*, 4177.

(45) De la Fuente, J. R.; Cañete, A.; Zanocco, A. L.; Saitz, C.; Jullian, C. *J. Org. Chem.* **2000**, *65*, 7949.

(46) Gan, H.; Whitten, D. G. *J. Am. Chem. Soc.* **1993**, *115*, 8031.

(47) Ci, X. H.; Kellett, M. A.; Whitten, D. G. *J. Am. Chem. Soc.* **1991**, *113*, 3893.

JP901877Q